A COMPARATIVE STUDY BETWEEN DWT AND DCT TRANSFORMS FOR COMPRESSED SENSING OF MOUSE ABDOMINAL MRI

Abstract — In this work, two different transformations are used alongside with the well-known compressed sensing methodology to evaluate the quality and time performance of image reconstruction using real magneto-resonance images from a mouse abdomen, namely, the discrete wavelet transform (DWT) and the discrete cosine transformation (DCT). For evaluating image quality, *k*-space data were subsampled using a pseudo-random variable density model with a reduction factor between $2-10$. The quantitative analysis of the reconstructed images was made by using Pearson's correlation coefficient calculated between the reference and reconstructed images. The results of image reconstruction using DWT and DCT presented similar Pearson's coefficient values for all acceleration rates indicating similarity above 0.90 between the reference and reconstructed images up to acceleration rate 6. Using DWT, a reduction between 79% and 85% of time spent on the image reconstruction was achieved. The experimental results show the efficiency of DWT as far as keeping similarity with the reference image in terms of correlation and on accelerating mouse abdominal MRI is concerned.

Keywords — Compressed sensing, subsampling pattern, small animal, Magnetic resonance imaging (MRI), variable density.

1 Introduction

Pre-clinical magnetic resonance imaging (MRI) of mice allows the investigation of several human-related pathologies (Driehuys et al., 2008). However, the imaging of pathologies located in the mice abdominal area involves the suppression of respiratory motion artifacts and requires long data acquisition time (Ehman et al., 1984; Farias et al., 2018). Additionally, MRI of small animals requires the use of anesthetic and the prolonged imaging time causes undesirable effects in the animal such as central nervous system depression, heart and respiratory rate decrease and hypothermia inside the cold magnet bore (Tremoleda et al., 2012). Therefore, to identify solutions that allow accelerating mouse abdominal image is of great interest since they will allow to reduce the image costs, to perform a greater number of preclinical assays and to minimize the suffering of the animal.

Conventionally, all *k*-space data in MRI is sampled and a Fast Fourier Transform is applied to the data for image reconstruction. However, due to physical and physiological limitations, a complete acquisition of the data requires a long acquisition time and new methods based on the reduction of acquired data have been developed (Budjan et al., 2016; Breuer et al., 2005; Pruessmann et al., 1999). A promising method to accelerate data acquisition is to use the Parallel Imaging technique (Deshmane et al., 2012). However, the need for additional hardware makes its application expensive in already installed scanners (Wech et al., 2011).

As an alternative, compressed Sensing - CS is a technique applied in MRI that promises to reduce *k*-space data by exploring the sparseness of images (Candes et al., 2006; Donoho, 2006) and, therefore, can potentially accelerate the image acquisition process. Due to the inherent sparsity of MRI, CS reconstruction can recover images from heavily subsampled MRI datasets. This image recovery relies on several critical conditions: First, the image must be accurately represented by a relatively small number of coefficients in a linear transform domain. Second, subsampling should produce incoherent aliasing artifacts in this transform domain. Lastly, a nonlinear algorithm should be used to simultaneously enforce the compressibility of reconstructed images and consistency of the reconstructions with the data acquired. A pseudo-random variable density *k*-space subsampling scheme is typically applied to ensure the artifact incoherence (Lustig et al., 2007). To reinforce image sparsity, data acquired directly from the scanner are projected on sparse transformed bases, usually, 2D discrete cosine transform – DCT (Ahmed et al., 1974) or 2D discrete wavelet transform – DWT (Elad, 2011). These transformations are commonly used in CS because it allows storing in a few coefficients all data image (Lustig et al., 2007). In a recent study, data from mouse abdominal MRI were acquired and subsampled up to $4\times$ using the DWT transform. It allowed a reduction of 62.5% in data acquisition time with an image similarity of 0.93 (Farias et al., 2018). In another study, a comparative study using different transformation bases for compressed sensing, both Peak Signal-to-Noise Ratio (PSNR) and Structural Similarity (SSIM) metrics showed a higher quality of MRI reconstruction using DWT than DCT transform (Mourchid and El Hassouni, 2015).

Considering that the most well-known image compression tools, DCT and DWT, adopt different codification methodology and that CS reconstruction quality should be verified for each application (Lustig et al., 2007), this study hypothesizes that the use of DWT and DCT transforms might present different CS reconstruction time for mouse abdominal image. Thus, this study proposes to investigate the performance of DWT and DCT transform by comparing the image quality and CS reconstruction time for mouse abdominal MRI. The result allows identifying the best transform which can be used in future works to accelerate mouse abdominal image. For comparison purposes, the reconstruction by CS uses only one pseudo-random variable density subsampling model with reduction factors between $2-10$. The results show that CS reconstruction using DWT and DCT transforms produce similar image quality in accordance with (Lustig et al., 2007), altought longer reconstruction time is identified for DCT.

Hereafter, the remainder of this paper is organized as follow. Section 2 describes the materials and methods used to evaluate the performance of the

DWT and DCT. Additionally, Section 2 details the reconstruction using CS, the MR data acquisition and the subsampling pattern adopted in this work. Section 3 presents the results and, finally, Section 4 presents the discussion.

2 Materials and Methods

2.1 Image Reconstruction

CS can be successfully applied to MRI based on the prior knowledge that the MRI images can be sparsely represented on an appropriate basis, such as DWT (Lustig et al., 2008). An image of length n has a sparse representation when it can be represented by $n \ll k$ sparse coefficients other than zero. Moreover, by applying the random subsampling scheme in k-space, the aliasing artifacts become incoherent distributed as random noise on the whole image and, consequently, an image can be recovered by using a nonlinear reconstruction algorithm. The algorithm which enforces the sparsity has the effect of making zero insignificant coefficients while maintaining the largest coefficients. Mathematically, the CS reconstruction can be formulated as the following constrained optimization problem (Motaal et al., 2013):

$$\min_{\mathrm{m}} \|(\mathcal{F}_u m - \mathrm{S})\|_2 + \lambda_1 \|\Phi_{\mathrm{m}}\|_1 + \lambda_2 \mathrm{TV(m)}, \quad (1)$$

where m symbolizes the reconstructed image and $\mathcal{F}_u$ the subsampled Fourier Transform. The first term of Eq. (1) enforces the data consistency taken into account $\ell_2 - norm$, penalizing the difference between reconstructed subsampled image ($\mathcal{F}_u m$) and k-space data image S, made available from the scanner. The second term promotes sparsity by $\ell_1 - norm$ minimizing the image data in the transformed domain Φ. The third term reduces noise and aliasing artifacts in the reconstructed image by penalizing the sum of spatial finite differences of the absolute total image variation, $TV(m)$.

In this study, CS reconstructions of subsampled MRI data were implemented using the wavelet (Daubechies 4) and DCT transforms, solving the optimization problem given in Eq. (1), using the nonlinear conjugate-gradient algorithm available in (Michael Lustig, Website accessed 02/07/2018). CS reconstruction quality is mainly determined by the sparsity and by the data image incoherency (Candes and Tao, 2006; Candes and Wakin, 2008). In this way, to achieve a good reconstruction performance an appropriate choice of parameters for each application should be made. Parameters λ_1 and λ_2 are utilized to minimize undesired loss of image features with low contrast and/or small size. Separate reconstructions were performed while $\lambda_{1,2}$ were independently varied from 0 to 50×10^{-6} in order to obtain the maximum image quality. The optimal penalty weights found were $\lambda_1 = \lambda_2 = 9 \times 10^{-6}$ which allowed highest image quality measured in terms of Pearson's correlation. The algorithm adopted in this work applies iterative thresholding. The number of algorithm iterations for iterative thresholding was calculated experimentally to reach the maximum image quality and shorter reconstruction time, and the results will be shown in Section 3.

2.2 MR image

The MRI data used in this work to evaluate the DWT and DCT performance by CS reconstruction was obtained from respiratory gating technique as described in (Farias et al., 2018). The fully sampled raw Fourier data with a resolution of 256×256 for reference image was obtained from the mouse abdomen in a $4.7\,Tesla$ scanner for small animals UNITYINOVA NMR (Agilent Technologies, 1998).

Pearson's correlation coefficient, ρ, is a formal correlation measure and is widely used in statistical analysis, pattern recognition and image processing (Charrier et al., 2010). It is a method for establishing the degree of probability that a linear relationship exists between two measured quantities. Typically, the agreement level between the reference and the reconstructed image is some measure of covariation between each one of them. In this work, the reconstructed images (subsampled) were evaluated by comparing their similarity to the reference image (fully sampled) using Pearson's correlation coefficient. For this, the middle lines from the reference and reconstructed images (on acceleration rates $2,3,\ldots,10$) were compared according to Eq. (2)

$$\rho_{X,Y} = \frac{cov(X,Y)}{\sigma_X \sigma_Y} \quad (2)$$

where X and Y are the middle lines of reference and reconstructed image respectively, cov is the covariance and σ_X and σ_Y are the standard deviation of X and Y respectively.

2.2 Subsampling Patterns

To accelerate MRI acquisition, it is necessary to reduce the number of phase-encoding data adopting an incoherent subsampling scheme. Finding an optimal sampling scheme that maximizes the incoherence for a given number of samples is a combinatorial optimization problem and might be considered intractable. A plausible choice is reducing the density according to a power of the distance from the origin. This study adopted a single subsampling pattern based on a pseudo-random variable-density subsampling in accordance with the Monte Carlo model as suggested in (Lustig et al., 2007; Farias et al., 2018).

Figure 1 shows an example of a pseudo-random subsampling pattern for acceleration rate 2. In a) it is shown the probability density function (pdf), b) shows the subsampled pattern generated and c) and d), respectively, the k-space and the subsampled k-space in accordance with b). In the subsampling pattern from b), the centre was densely sampled, decreasing the density in accordance with the pdf in a).

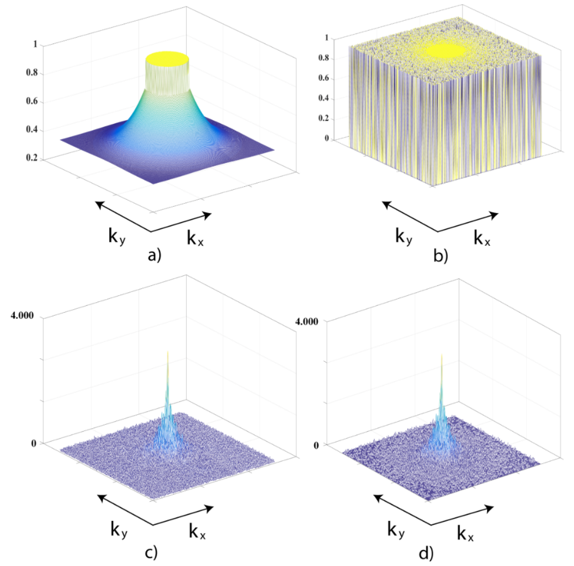

Figure 1 – Example of a subsampled pattern for acceleration rate 2 based on Monte Carlo method. The pattern kept the centre densely sampled. a) probability density function, b) example of pseudo-random variable-density subsampling, c) *k*-space fully sampled and d) *k*-space subsampled in accordance to b). Samples corresponding to blue points on the top of b) are not acquired in *k*-space.

The sample patterns for each acceleration rate were generated and multiplied by fully sample data to get the following amount of data: 2 (50% of data); 3 (33% of data); 4 (25% of data); 5 (20% of data); 6 (17% of data); 7 (14% of data); 8 (12% of data); 9 (11% of data); and 10 (10% of data). The ideal sample incoherence for each acceleration rate was selected among 2000 candidates based on maximum sample incoherence calculated by the standard deviation of the sidelobe-to-peak ratio in accordance to (Lustig et al., 2007; Farias et al., 2018). The incoherence values for each acceleration rate is shown in Figure 2.

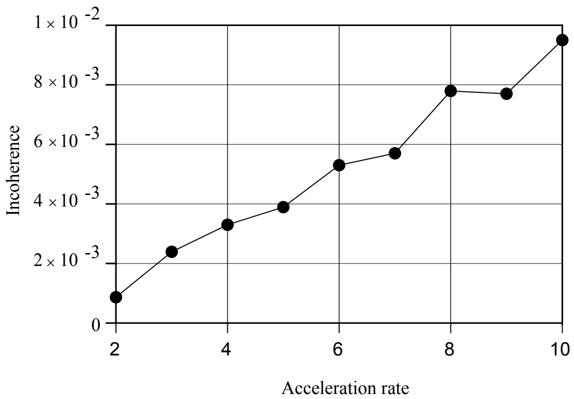

Figure 2 – Sample pattern incoherence values for acceleration rate $2-10$.

3 Results

Figure 3 shows the reconstruction time results by CS using the DWT and DCT transforms as well as the Pearson's correlation coefficient values for acceleration rate $2, 4, 6, 8$ and 10, on iterations $1, 10, 20$ and 30. The results in the figure show the occurrence of a reduction in the reconstruction time by CS using DWT between 79% and 85% keeping almost the same correlation coefficient that DCT's. The reconstruction time is higher for higher values of algorithm iterations for both DWT and DCT transforms. Moreover, the use of only one iteration indicates low computational cost and equal image coefficient values for each acceleration rate for both DWT and DCT transforms. Hereafter, for comparison purposes, this study adopted only one iteration to evaluate the quality of CS reconstruction using CS-DWT and CS-DCT.

The subsampled images reconstructed by CS-DWT and CS-DCT on acceleration rates $2-10$ were implemented to have their results subjectively compared. Figure 4 shows the reference image on the top panel and the images reconstructed by CS adopting DWT and DCT transforms on the bottom panels. It is noticeable in all reconstructed images that CS-DWT and CS-DCT exhibit visually the same quality. Additionally, the images from acceleration rates 8 and 10 show blurred features due to aliasing artifact errors (pointed out by an arrow in the figure).

In order to objectively demonstrate the similarity of CS reconstruction from subsampled k-space for all acceleration rates, centre lines from the reference and reconstructed images in acceleration rates $2-10$ were analyzed using the Pearson's correlation test as can be seen in Figure 5. As the acceleration rate increases, the Pearson's coefficients from CS reconstructed images adopting DWT and DCT transforms decreases from 0.958 on acceleration rate 2 to 0.83 on acceleration rate 10. Additionally, both transforms show small differences between Pearson's coefficient values for almost all acceleration rates.

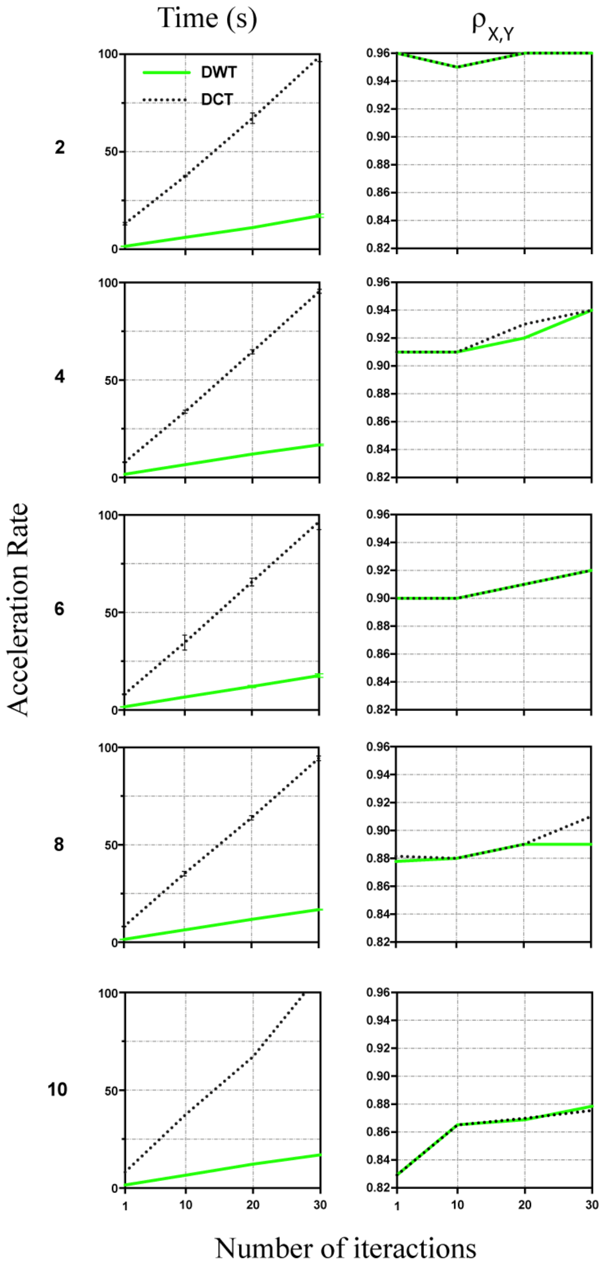

Figure 3 - Reconstruction time by CS using DWT and DCT as a function of the number of iterations and their respective Pearson's coefficients at acceleration rates 2, 4, 6, 8 and 10. The figure indicates lower reconstruction times for DWT and longer for DCT reconstruction at acceleration rates 2, 4, 6, 8 and 10.

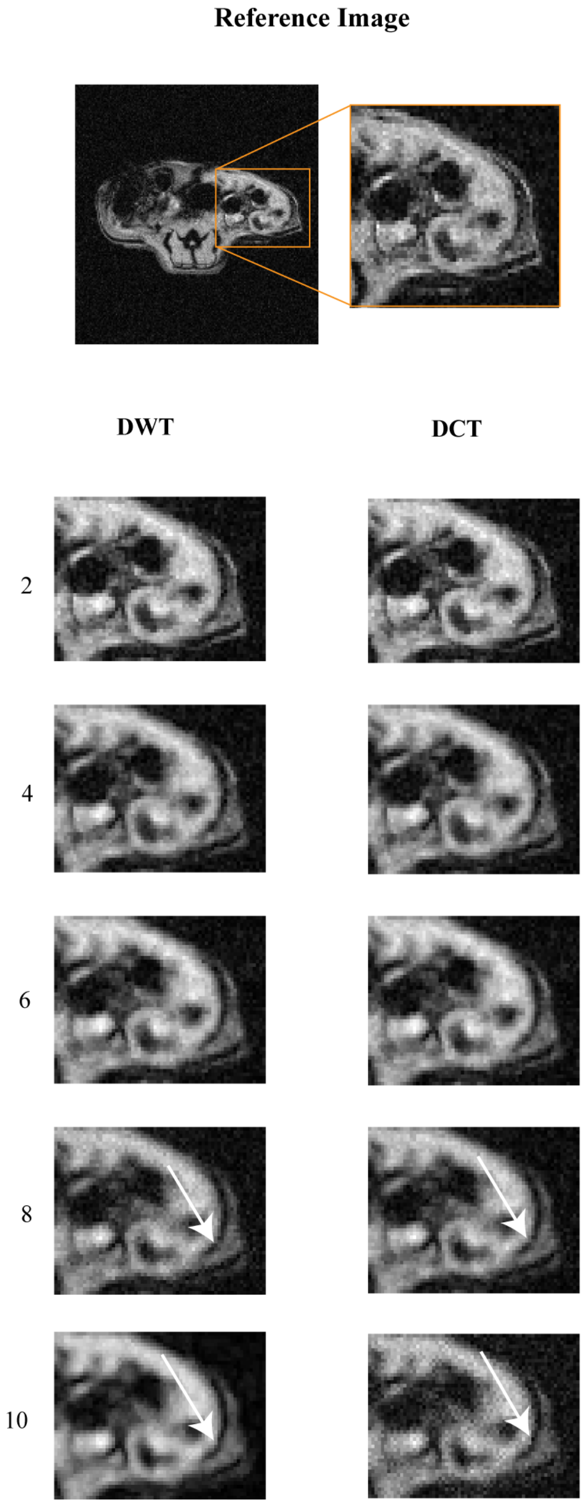

Figure 4 – Reference image and the subsampled image reconstructed by CS adopting DWT and DCT on acceleration rates 2, 4, 6, 8 and 10. The images 8 and 10 are blurred by aliasing artifact errors (pointed out by arrow).

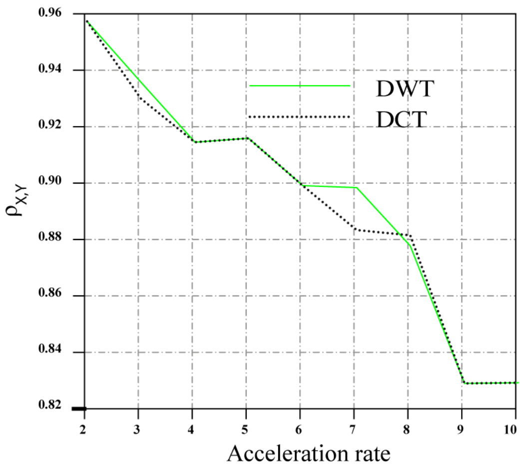

Figure 5 – Pearson's coefficient, $\rho_{X,Y}$, between the reference and reconstructed images by CS adopting DWT and DCT transforms on acceleration rates $2-10$. Coefficient values higher than 0.90 indicate a strong correlation between reference and reconstructed images.

4 Discussion

In this study, the *k*-space is experimentally subsampled by a pseudo-random variable density scheme in order to compare the image correlations and reconstruction time by CS adopting DWT and DCT transforms.

Pearson's correlation values larger than 0.90 indicate a significant correlation between the reference and reconstructed images. This means that the reconstructed images maintain an almost optimal image agreement by preserving details of image structure. On the other hand, a reduced correlation value means that the reconstructed images are blurred with aliasing artifacts introduced by data subsampling which could not be removed by CS reconstruction. Therefore, this study considers acceleration rate up to 6 as the best image reconstruction for both DWT and DCT transforms.

The Pearson's correlation coefficient for images reconstructed using CS-DWT and CS-DCT was similar for almost all iterations between $1-30$. However, the image reconstruction time using CS-DWT was significantly smaller than CS-DCT's for all iterations values. This result can be attributed to the greater sparsity of CS-DCT which, because its smaller amount of coefficients, offers a higher efficiency in CS reconstruction (Gomes et al., 2013; Bruckstein et al., 2009).

For future work, the results presented here should be compared to the ones using other sample patterns such as radial (Rasche et al., 1994) and spiral (Liao et al., 1997) sample. Despite the fact that only one mouse was used in this work, the performance of DWT and DCT transforms in CS reconstruction for mouse abdominal image could be evaluated by using the results presented here.

4 Conclusion

This study aimed to compare the quality and time of CS reconstruction using DCT and DWT transforms in abdominal mouse MRI accelerated between $2-10$. Based upon the results presented, it can be concluded that CS-DWT transform produces a reduction in the image reconstruction time between 79% and 85% that keeps the correlation with reference image higher than 0.90 up to acceleration rate 6. Considering the constant need to reduce costs in pre-clinical MRI, this study demonstrated that using DWT transform in CS reconstruction of mouse abdominal image allows a shorter reconstruction time. Additionally, the shorter times for DWT transform may reduce the image cost and the animal suffering due to its less exposure to the deleterious effects of the anesthetic.

Acknowledgments:

This work has been supported by the Brazilian agency CAPES, CEFET-MG, CNPq, and FAPEMIG.

References

Ahmed, N., Natarajan, T. & Rao, K. R. 1974. Discrete cosine transform. *IEEE transactions on Computers,* 100(1), pp 90-93.

Breuer, F. A., Kellman, P., Griswold, M. A. & Jakob, P. M. 2005. Dynamic autocalibrated parallel imaging using temporal GRAPPA (TGRAPPA). *Magnetic resonance in medicine,* 53(4), pp 981-985.

Bruckstein, A. M., Donoho, D. L. & Elad, M. 2009. From sparse solutions of systems of equations to sparse modeling of signals and images. *SIAM review,* 51(1), pp 34-81.

Budjan, J., Schoenberg, S. O. & Riffel, P. 2016. Fast Abdominal Magnetic Resonance Imaging. *Rofo,* 188(6), pp 551-8.

Candes, E. J., Romberg, J. & Tao, T. 2006. Robust uncertainty principles: exact signal reconstruction from highly incomplete frequency information. *IEEE Transactions on Information Theory,* 52(2), pp 489-509.

Candes, E. J. & Tao, T. 2006. Near-Optimal Signal Recovery From Random Projections: Universal Encoding Strategies? *IEEE Transactions on Information Theory,* 52(12), pp 5406-5425.

Candes, E. J. & Wakin, M. B. 2008. An Introduction To Compressive Sampling. *IEEE Signal Processing Magazine,* 25(2), pp 21-30.

Charrier, C., Knoblauch, K., Moorthy, A. K., Bovik, A. C. & Maloney, L. T. Comparison of image quality assessment algorithms on compressed images. Image Quality and System Performance VII, 2010. International Society for Optics and Photonics, 75290B.

Deshmane, A., Gulani, V., Griswold, M. A. & Seiberlich, N. 2012. Parallel MR imaging. *J Magn Reson Imaging,* 36(1)**,** pp 55-72.

Donoho, D. L. 2006. Compressed sensing. *IEEE Transactions on Information Theory,* 52(4)**,** pp 1289-1306.

Driehuys, B., Nouls, J., Badea, A., Bucholz, E., Ghaghada, K., Petiet, A. & Hedlund, L. W. 2008. Small animal imaging with magnetic resonance microscopy. *ILAR J,* 49(1)**,** pp 35-53.

Ehman, R. L., McNamara, M. T., Pallack, M., Hricak, H. & Higgins, C. B. 1984. Magnetic resonance imaging with respiratory gating: techniques and advantages. *AJR Am J Roentgenol,* 143(6)**,** pp 1175-82.

Elad, M. 2011. *Sparse and Redundant Representations: From Theory to Applications in Signal and Image Processing*, New York.

Farias, A. R., de Castro Medeiros, D., Magalhães, H. A., Moraes, M. F. D. & Mendes, E. M. 2018. A novel approach for accelerating mouse abdominal MRI by combining respiratory gating and compressed sensing. *Magnetic Resonance Imaging*.

Gomes, J., Levy, S. & Velho, L. 2013. *Image Processing for Computer Graphics*: Springer New York.

Liao, J. R., Pauly, J. M., Brosnan, T. J. & Pelc, N. J. 1997. Reduction of motion artifacts in cine MRI using variable-density spiral trajectories. *Magn Reson Med,* 37(4)**,** pp 569-75.

Lustig, M., Donoho, D. & Pauly, J. M. 2007. Sparse MRI: The application of compressed sensing for rapid MR imaging. *Magn Reson Med,* 58(6)**,** pp 1182-95.

Lustig, M., Donoho, D. L., Santos, J. M. & Pauly, J. M. 2008. Compressed Sensing MRI. *IEEE Signal Processing Magazine,* 25(2)**,** pp 72-82.

Michael Lustig, e. a. Website accessed 02/07/2018. *SparseMRI V0.2* [Online]. Available: http://people.eecs.berkeley.edu/~mlustig/Software.html.

Motaal, A. G., Coolen, B. F., Abdurrachim, D., Castro, R. M., Prompers, J. J., Florack, L. M., Nicolay, K. & Strijkers, G. J. 2013. Accelerated high-frame-rate mouse heart cine-MRI using compressed sensing reconstruction. *NMR Biomed,* 26(4)**,** pp 451-7.

Mourchid, Y. & El Hassouni, M. Comparative study between different bases of transformation for compressive sensing of images. Intelligent Systems and Computer Vision (ISCV), 2015, 2015. IEEE, 1-7.

Pruessmann, K. P., Weiger, M., Scheidegger, M. B. & Boesiger, P. 1999. SENSE: sensitivity encoding for fast MRI. *Magn Reson Med,* 42(5)**,** pp 952-62.

Rasche, V., Holz, D. & Schepper, W. 1994. Radial turbo spin echo imaging. *Magn Reson Med,* 32(5)**,** pp 629-38.

Tremoleda, J. L., Kerton, A. & Gsell, W. 2012. Anaesthesia and physiological monitoring during in vivo imaging of laboratory rodents: considerations on experimental outcomes and animal welfare. *EJNMMI Res,* 2(1)**,** pp 44.

Wech, T., Lemke, A., Medway, D., Stork, L. A., Lygate, C. A., Neubauer, S., Kostler, H. & Schneider, J. E. 2011. Accelerating cine-MR imaging in mouse hearts using compressed sensing. *J Magn Reson Imaging,* 34(5)**,** pp 1072-9.